Neuroscience 140 (2006) 123–136

MORPHOLOGICAL PROPERTIES OF MOUSE RETINAL GANGLION CELLS

J. COOMBS,[a] D. VAN DER LIST,[a] G.-Y. WANG[d] AND L. M. CHALUPA[a,b,c]*

[a]*Section of Neurobiology, Physiology and Behavior, College of Biological Sciences, University of California, One Shields Avenue, Davis, CA 95616, USA*

[b]*Center for Neuroscience, University of California, Davis, CA 95616, USA*

[c]*Department of Ophthalmology, School of Medicine, University of California, Davis, CA 95616, USA*

[d]*Department of Structural and Cellular Biology, Tulane University School of Medicine, New Orleans, LA 70112, USA*

Abstract—The mouse retina offers an increasingly valuable model for vision research given the possibilities for genetic manipulation. Here we assess how the structural properties of mouse retinal ganglion cells relate to the stratification pattern of the dendrites of these neurons within the inner plexiform layer. For this purpose, we used 14 morphological measures to classify mouse retinal ganglion cells parametrically into different clusters. Retinal ganglion cells were labeled in one of three ways: Lucifer Yellow injection, 'DiOlistics' or transgenic expression of yellow fluorescent protein. The resulting analysis of 182 cells revealed 10 clusters of monostratified cells, with dendrites confined to either On or Off sublaminae of the inner plexiform layer, and four clusters of bistratified cells, dendrites spanning the On and Off sublaminae. We also sought to establish how these parametrically identified retinal ganglion cell clusters relate to cell types identified previously on the basis of immunocytochemical staining and the expression of yellow fluorescent protein. Cells labeled with an antibody against melanopsin were found to be located within a single cluster, while those labeled with the SMI-32 antibody were in four different clusters. Yellow fluorescent protein expressing cells were distributed within 13 of the 14 clusters identified here, which demonstrates that yellow fluorescent protein expression is a useful method for labeling virtually the entire population of mouse retinal ganglion cells. Collectively, these findings provide a valuable baseline for future studies dealing with the effects of genetic mutations on the morphological development of these neurons.

Key words: cluster analysis, cell classification, retina, multivariate analysis, dendrites.

*Correspondence to: L. M. Chalupa, Section of Neurobiology, Physiology and Behavior, College of Biological Sciences, University of California, One Shields Avenue, Davis, CA 95616, USA.
E-mail address: lmchalupa@ucdavis.edu (L. M. Chalupa).

Abbreviations: AP, alkaline phosphatase; EMEM, Eagle's minimum essential medium; GCL, ganglion cell layer; GFP, green fluorescent protein; INL, inner nuclear layer; IPL, inner plexiform layer; LY, Lucifer Yellow; PBS, phosphate-buffered saline; PFA, paraformaldehyde; RGC, retinal ganglion cell; Thy-1, thymus cell antigen 1; YFP, yellow fluorescent protein.

Retinal ganglion cells (RGCs) have been categorized into different classes in a number of species including, monkey (Perry and Cowey, 1984; Perry et al., 1984; Rodieck and Watanabe, 1993; Dacey et al., 2003), cat (Boycott and Wassle, 1974; Stone and Clarke, 1980; Berson et al., 1998, 1999; Isayama et al., 2000), ferret (Vitek et al., 1985; Wingate et al., 1992), rabbit (Amthor et al., 1983; Marc and Jones, 2002; Rockhill et al., 2002), rat (Perry, 1979; Peichl, 1989; Huxlin and Goodchild, 1997; Sun et al., 2002b), and mouse (Doi et al., 1995; Sun et al., 2002a; Badea and Nathans, 2004; Kong et al., 2005). The morphological criteria commonly employed to classify ganglion cells have been soma size and dendritic field dimensions. In certain species, this approach has been validated by functional data as well as by the demonstration that different ganglion cell classes project to different retinorecipient targets (Saito, 1983; Leventhal et al., 1985; Berson et al., 1998, 1999; Isayama et al., 2000; Kaplan, 2004). In cat and monkey, morphological differences between RGC classes are quite pronounced so that reliance on soma and dendritic field size is generally sufficient to categorize cells into major classes. But even in these species, more refined criteria are required for a finer-grained analysis of RGC classes (Kolb et al., 1981; Rodieck and Watanabe, 1993; Berson et al., 1998, 1999; Isayama et al., 2000; Dacey et al., 2003).

Studies of the rat (Huxlin and Goodchild, 1997; Sun et al., 2002b) and mouse (Sun et al., 2002a) retina have shown that with the exception of the largest ganglion cells, considered homologous to the alpha cells first identified in the cat (Peichl, 1991), there is considerable overlap in both soma and dendritic field measurements of RGCs in these rodents. Two recent papers have defined classes of mouse RGCs on the basis of quantitative measurements. Badea and Nathans (2004) provided a cluster analysis of retinal interneurons as well as ganglion cells in the mouse. These authors relied on a genetically directed promotor, alkaline phosphatase (AP) to visualize the neurons they studied. A cluster analysis of mouse RGCs has been also provided by Kong et al. (2005) who relied on several different methods to label cells.

In the present study, we have extended the cluster analysis approach to the study of mouse RGCs. The approach we have taken involved making 14 different quantitative measures of structural properties with a subsequent cluster analysis that defined 14 different groupings of cells. We then assessed how these related to the stratification patterns exhibited by the dendrites of these neurons within the inner plexiform layer (IPL). In addition, we sought to establish how these parametrically identified

0306-4522/06$30.00+0.00
doi:10.1016/j.neuroscience.2006.02.079

RGC clusters relate to cells types identified previously on the basis of immunocytochemical labeling for melanopsin (Provencio et al., 2000; Belenky et al., 2003) and SMI-32, an antibody against neurofilament H (Lin et al., 2004), as well as ganglion cells expressing yellow fluorescent protein (YFP) in transgenic mice (Feng et al., 2000).

EXPERIMENTAL PROCEDURES

Animal and tissue preparation

Retinas from C57BL/6 mice and transgenic mice expressing YFP controlled by a Thy-1 (thymus cell antigen 1) regulator on a C57 background (YFP-H line, Jackson Laboratory, Bar Harbor, ME, USA; Feng et al., 2000) were studied. A lethal dose of Euthana-6 (0.2 ml, pentobarbital sodium, Western Medical Supply Inc., Arcadia, CA, USA) was administered before retinal removal. The retinas were marked either temporally or nasally, isolated and placed in either Eagle's minimum essential medium (EMEM, Sigma Chemical Co., St. Louis, MO, USA) or 4% paraformaldehyde (PFA, Sigma) in phosphate-buffered saline (PBS, EM Science, Gibbstown, NJ, USA) depending on the labeling method.

Labeling techniques

Mouse RGCs were labeled in one of four ways: i) intracellular injections of Lucifer Yellow (LY); ii) DiOlistics (Gan et al., 2000), iii) expression of transgenic YFP, or iv) by immunocytochemistry. For LY injections, retinas were isolated, cut into nasal and temporal halves, and mounted on filter paper (0.45 μm, Millipore), then placed in a chamber perfused with EMEM, continuously bubbled with 95% oxygen and 5% carbon dioxide, on an upright microscope (Nikon, Garden City, NY, USA) equipped with Nomarski optics and long working-distance objectives. Sharp electrodes (borosilicate glass, Sutter Instrument Co., Novato, CA, USA) were pulled on a Flaming/Brown micropipette puller (Sutter Instrument Co.) and filled with 5–7 mM LY (lithium salt, Molecular Probes, Eugene, OR, USA) in 20 mM MOPS. Electrodes were visually inserted into cell bodies in the ganglion cell layer (GCL) and current was applied to fill cells with LY. One to four non-overlapping cells were typically filled per retinal half, after which the tissue was immediately transferred to 4% PFA in a foil-covered vial and refrigerated at 4 °C. After 12 h retinas were placed in PBS. For DiOlistics labeling (Gan et al., 2000), tungsten particles (1.1–1.7 μm, Bio-Rad Laboratories, Hercules, CA, USA) were coated with 1,1′-dioctadecyl-3,3,3′,3′-tetramethylindocarbocyanine perchlorate (DiI) or 3,3′-dioctadecyloxacarbocyanine perchlorate (DiO) and propelled into the GCL of a retinal whole mount using a gene gun (Helios Gene Gun, Bio-Rad Laboratories) with helium gas as the propellant. For fresh tissue, retinas were dissected out in EMEM and flattened on a piece of filter paper for shooting (at 100–140 p.s.i. helium). The tissue was then incubated for 15–45 min at room temperature in oxygenated EMEM before being placed in a vial of 4% PFA and refrigerated overnight. For fixed tissue, retinas were isolated and flattened on a piece of filter paper for shooting (140–170 p.s.i. helium) and then placed in a foil-covered vial of PBS for up 3 days at room temperature. Retinas of transgenic mice expressing YFP were removed, fixed for 1–2 h in PFA, mounted on a slide and visualized. In some cases YFP expression was enhanced for imaging purposes by using rabbit anti-green fluorescent protein (GFP) (1:500, Molecular Probes). The whole mount preparation was as follows: Fixed retinas were blocked for 2 h in a solution containing 10% normal donkey serum, 2% bovine serum albumen, 0.3% Triton X-100 in PBS. The retinas were then incubated in the primary antibody for 3–4 days at 4 °C in blocking solution, then washed in PBS before incubating in CY3 secondary (1:500; Jackson ImmunoResearch Laboratory., Inc., West Grove, PA, USA) for 3 h, and finally washed again before being mounted in PBS.

Immunocytochemistry

Melanopsin-containing cells were labeled using an antibody against mouse melanopsin (a generous gift from I. Provencio; Provencio et al., 2000; Belenky et al., 2003). A goat anti-rabbit TSA kit (Molecular Probes) was used to amplify the signal. Whole mount retinas were quenched in 2% hydrogen peroxide in PBS for 30 min, then washed well in PBS and placed in blocking buffer with 0.1% Triton X-100 overnight. The tissue was then incubated in mouse melanopsin antibody (1:5000 dilution) in blocking buffer for 5–7 days at 4 °C, washed in PBS, and then placed in horseradish peroxidase (1:100) in blocking buffer for 4 h at room temperature. The signal was detected using tyramide–Alexafluor (1:500) in amplification buffer with 0.0015% hydrogen peroxide for 30 min at room temperature. Cells expressing a non-phosphorylated epitope in neurofilament H were visualized by the co-localization of YFP-expressing RGCs in transgenic mice with anti-SMI-32 label, a monoclonal antibody to neurofilaments (Lin et al., 2004), purchased from Sternburger Monoclonals, MD, USA. The whole mount preparation was as follows: Fixed retinas were blocked for 2 h in a solution of 10% normal donkey serum, 2% bovine serum albumen, and 0.3% Triton X-100 in PBS. The retinas were then incubated in primary antibody (1:100) for 3–4 days at 4 °C in blocking solution, washed in PBS, incubated in CY3 secondary (1:500; Jackson ImmunoResearch Laboratories) for 2 h, and washed again in PBS before visualization.

Imaging and morphometric measures

Retinal tissue was first visualized on an upright epifluorescence microscope (Nikon) to locate labeled RGCs and document their loci. Only cells with obvious axons were studied. Using an Olympus Fluoview 300 or 500 confocal microscope, high-resolution three-dimensional images were made of each cell (x and y= 1024×1024 pixels, with two to three images averaged at each focal plane). Scans were taken at 0.25–0.7 μm intervals along the *z* axis depending on the objective used. Each confocal image was traced using Neurolucida software (Microbrightfield, Inc., Colchester, VT, USA), and the following parameters were measured: (i) Somal size: a topographic series of contour lines were drawn around each soma to outline the shape in three-dimensions with the largest contour used to calculate the area. (ii) Dendritic field size: a line was drawn connecting the outermost tips of the dendrites around the edge of the arbor with dendritic field area defined as the area within this contour. (iii) Total dendrite length: the sum of the lengths of all the dendrites. (iv) Number of dendritic branches: all branches of all dendrites per cell. (v) Branch order: the largest number of times a dendrite branches, with the primary branch emerging from the soma defined as branch order 1. (vi) Mean internal branch length: average distance along the dendrite between the soma and the first branch point and between branch points. (vii) Mean terminal branch length: average distance along the dendrite from the last branch point to the end of the dendrite. (viii) Branch angle: the angle (in three-dimensions) formed by two lines that each pass through the branch point and the two subsequent branch points. (ix) Number of dendrites: number of primary dendrites emerging from the soma. (x) Spine density: the total number of spines divided by the total dendrite length. (xi) Axon diameter: the mean diameter of the 100–300 μm segment nearest the soma. (xii) Dendrite diameter: the mean diameter of the three branch orders closest to the soma. (xiii) Tortuosity: the ratio of the length along each dendritic branch and the length of the straight line drawn between the two nodes that define the branch. (xiv) Symmetry: location of the soma in relation to the dendritic field from a bird's-eye view, expressed as a percentage of the radius of the dendritic field and the distance of the soma from the closest edge of the dendritic field. (xv) Stratification of dendrites: the location of the dendritic terminals within the IPL. The IPL was subdivided into five layers of equivalent width: two Off (layers 1

and 2, nearest the INL) and three On (layers 3–5, nearest the GCL). The boundaries of the IPL were visualized by labeling nuclei with DAPI (1:500 in PBS) overnight or by enhancing the contrast of the final image to highlight nuclei. The contrast of the final images was enhanced using Photoshop software (Adobe Systems, Inc.).

Statistical analyses

A cluster analysis ('joining' or tree method) was performed using 14 of the morphometric parameters listed above using Statistica software (StatSoft, Inc., Tulsa, OK, USA). These parameters were standardized (using means and standard deviations) so that the larger scaled measurements would not unduly influence the outcome. Parameters not showing a normal frequency distribution were first transformed to obtain a more symmetric distribution which enhanced the power of the analysis. For the monostratified cells, three parameters had normal distributions (dendrite length, branch angle, and dendrite diameter), four parameters were log transformed (dendritic field area, the internal and terminal branch lengths, and tortuosity) and seven were transformed using their square roots (soma area, number of dendrites, branch order, number of branches, spine density, axon diameter, and symmetry). For bistratified cells, two variables showed a normal distribution (dendrite length and branch angle), four were log transformed (tortuosity, dendrite and axon diameter, and dendritic field area) and seven were transformed using square roots (soma area, number of dendrites and branches, branch order, internal and terminal branch lengths, spine density, and symmetry).

There are two main ways to perform cluster analyses. One approach requires the number of clusters to be known beforehand. This analysis places items (i.e. cells) into a predetermined number of groups, minimizing differences within a cluster and maximizing differences between clusters (K-means method). The advantage of this method is that it produces *F*-values which indicate difference significances. The disadvantage is that one needs to know the number of clusters present in the population before the analysis is started. The other method, which we employed here, works well if the aim of the analysis is to determine the number of clusters present in the population. In this type of analysis (the joining or hierarchical method), each cell is defined initially as its own cluster and is then grouped with other cells or clusters in a stepwise fashion based on similarity. Those cells closest to each other in the multidimensional space (defined in this case by 14 measures) are grouped together earlier in the analysis than those that are further apart or less similar. This analysis creates a tree (or dendrogram) in which the shorter branches indicate larger similarities between individual cells or clusters. The distances (or dissimilarities) were initially defined by the absolute distance between cells in the multidimensional space (city-block distance). After the initial clusters were formed, distances between groups of cells were evaluated using an incremental sum of squares approach (Ward's method).

RESULTS

Mouse retina contains 14 clusters of RGCs

A total of 182 cells were included in this study: 72 were labeled using DiOlistics, 16 injected with LY, 84 expressed YFP, and 10 were labeled using the melanopsin antibody. Of the 182 RGCs in our sample, 133 were monostratified (dendrites confined to either the On or the Off sublamina of the IPL) and 49 were bistratified (dendrites spanning On and Off sublaminae). A cluster analysis was performed on each of these two cell classes, with the resulting dendrograms depicted in Fig. 1. To determine where to draw the line on the *y* axis defining discrete cell groupings, the linkage distance (a measure of dissimilarity) for each successive clustering step was plotted for both the mono- and bistratified cells. A sharp rise in the linkage distance (plotted on the *y* axis) indicated an abrupt increase in differ-

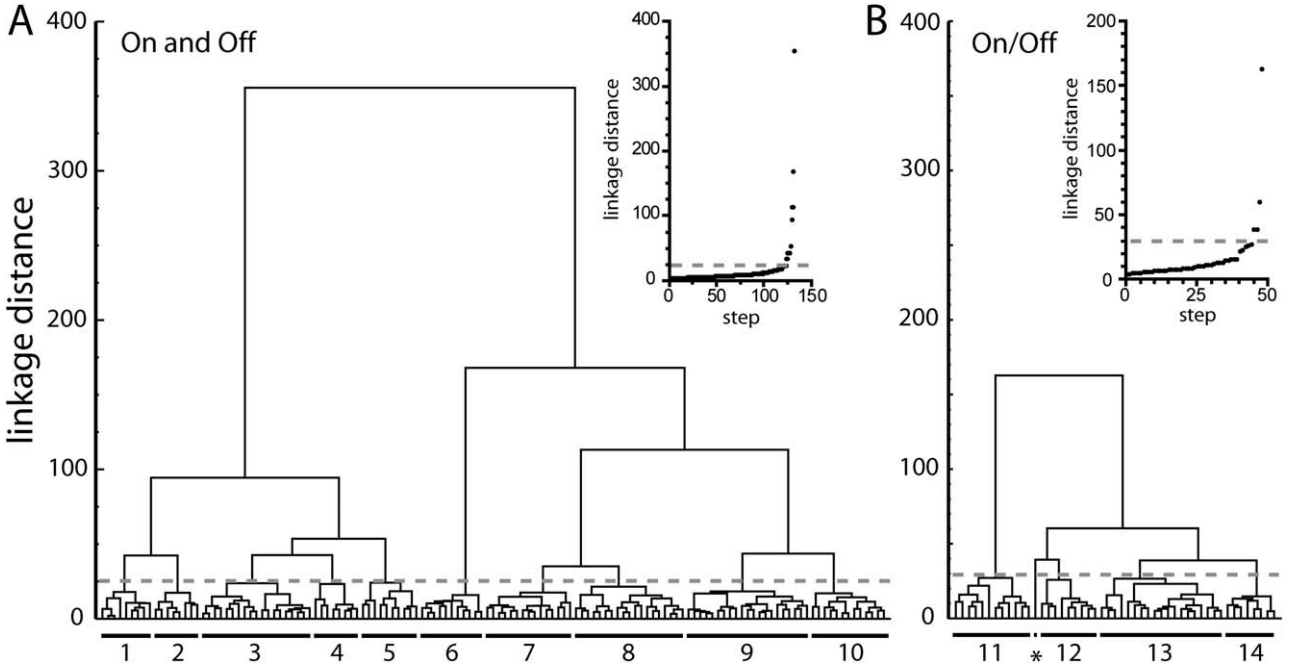

Fig. 1. Cluster analysis trees. Linkage distance (*y* axis) shows the relative similarity of cells (*x* axis) for monostratified (A) and bistratified cells (B). Step diagrams for each analysis (insets) plot the linkage distance of each clustering step, starting with cells that are most alike. The gray lines indicate abrupt increases in dissimilarity. Cells linked together below the gray lines are defined as cell types and given group numbers (shown under the trees). One cell forms its own cluster (* in B) and is not given a group name.

Table 1. The number of cells in the 14 clusters that were identified using four labeling methods

Label method	Monostratified clusters										Bistratified clusters					Total
	1	2	3	4	5	6	7	8	9	10	11	12	13	14	*	
DiI or DiO	6	6	4	6	5	—	6	4	4	4	12	4	8	3	—	72
LY	1	1	—	—	4	—	1	1	—	1	—	3	2	2	—	16
YFP (alone)	2	1	13	2	1	1	5	13	15	5	—	2	9	3	1	73
anti-melanopsin	—	—	—	—	—	10	—	—	—	—	—	—	—	—	—	10
YFP+SMI-32	—	—	2	—	—	—	4	—	2	3	—	—	—	—	—	11
Total	9	8	19	8	10	11	16	18	21	13	12	9	19	8	1	182

ences between cell groups. This value was the cutoff point below which cells were considered to be sufficiently alike to define single clusters. In these plots (insets in Fig. 1), the transition from small to large linkage distances is readily apparent and is indicated by the broken lines in both the insets and dendrograms. Clusters below this line were considered to represent discrete groups of RGCs. Using this approach, 14 separate classes of RGCs can be differentiated in the mouse retina. Ten of these are monostratified (clusters 1–10) and four are bistratified (clusters 11–14), as delineated by the numbers under each tree. We have designated these clusters M1–M14 (M for mouse). Table 1 shows the number of cells in the 14 clusters that were identified using the four different labeling methods employed in this study. Cells for different regions of the retina were grouped together since we did not observe any obvious differences in morphology with retinal eccentricity.

There was one bistratified 'cluster' that contained only one cell (* in Fig. 1B), and thus was not assigned a cluster name. This one cell looked different than the other bistratified cells, but was similar in appearance to the melanopsin-positive cells in the monostratified group.

Tracings of representative cells in Fig. 2 and 3 illustrate the similarities in size, shape, and branching patterns within each of the resulting clusters, with monostratified and bistratified cells shown respectively in the two figures. The tracings point out some clear properties that define the resulting groups. For instance, both clusters M1 and M2 are characterized by small dendritic fields, but the dendritic branching was more profuse in M1. Also, clusters M4 and M5 both contained asymmetric cells, but dendritic branching patterns were very different in the two groups. Examples of both On and Off cells are shown for three different clusters: M3, M7, and M9. In the M9 cluster, On and Off cells looked nearly identical, while in the M3 cluster, Off dendritic fields were smaller, and in M7, Off cells had dendrites that were appreciably less tortuous.

The analysis proved to be quite powerful as is evident in Figs. 2 and 3; however, because of the relatively small number of cells used to define a fairly large number of resulting cell clusters, we found that a few clusters contained cells that may define more than one cell type. We kept these RGCs in their respective clusters because the links were situated below the cutoff line in the dendrogram. Cells in cluster M4 showed two rather distinct morphologies. Examples from each of these groups (called 4a and 4b) are shown in Fig. 2. Cells in 4b (grouped together on the left side of cluster M4 in the dendrogram) showed unusually dense dendritic fields and had the longest total dendritic length of the RGCs studied. Cluster M5 also appeared to be composed of two types of cells. An asymmetric dendritic field characterized most cluster M5 cells, but there were three cells in this cluster that did not show the 'windblown' appearance evident in most M5 cells (see Fig. 2). These three 'odd' cells had dendrites that ramified in the central portion of the IPL, rather than in layer 1, near the inner nuclear layer (INL), which was characteristic of the other M5 cells.

Fig. 4 shows dendritic field diameters and soma sizes of the entire sample of cells studied. Note that there are no obvious groupings of cells in this overall distribution. However, certain clusters could be differentiated from the overall sample on the basis of these two conventional size measurements. Thus, RGCs with the largest dendritic fields were in clusters M6 (indicated by stars) and M10 (indicated by filled circles). Cluster M6 contained all the melanopsin-positive cells, as well as one YFP-expressing cell, while cells in M10 appeared equivalent to the alpha-type RGCs of other species (Peichl et al., 1987; Peichl, 1991). The smallest cells in our sample were the bistratified cells in cluster M11 (indicated by triangles).

Though many cells in M6, M10 and M11 may be identified on the basis of their dendritic field and soma sizes alone, there was enough overlap of these parameters between different clusters that these two measures by themselves were not sufficiently useful to distinguish among the cell clusters. For instance, clusters M1, M2, and M11 all had similar small dendritic fields and somas (see Fig. 5a and b, respectively). And though, the cells in cluster M11 were bistratified and distinguishable on this basis, size alone was not sufficient to separate M1, M2, and M11. Yet, the cells in these groups looked very different (see Figs. 2 and 3), thus other parameters were needed to tell them apart.

Dendritic stratification patterns

Fig. 6 shows images of cells from each of the 14 clusters from a bird's-eye view (XY plane) and from the side (XZ plane) to illustrate how the dendrites of these neurons ramify in the IPL. Note that these images are at different scales so as to emphasize differences in dendritic structure rather than size. The dendritic locations in the IPL

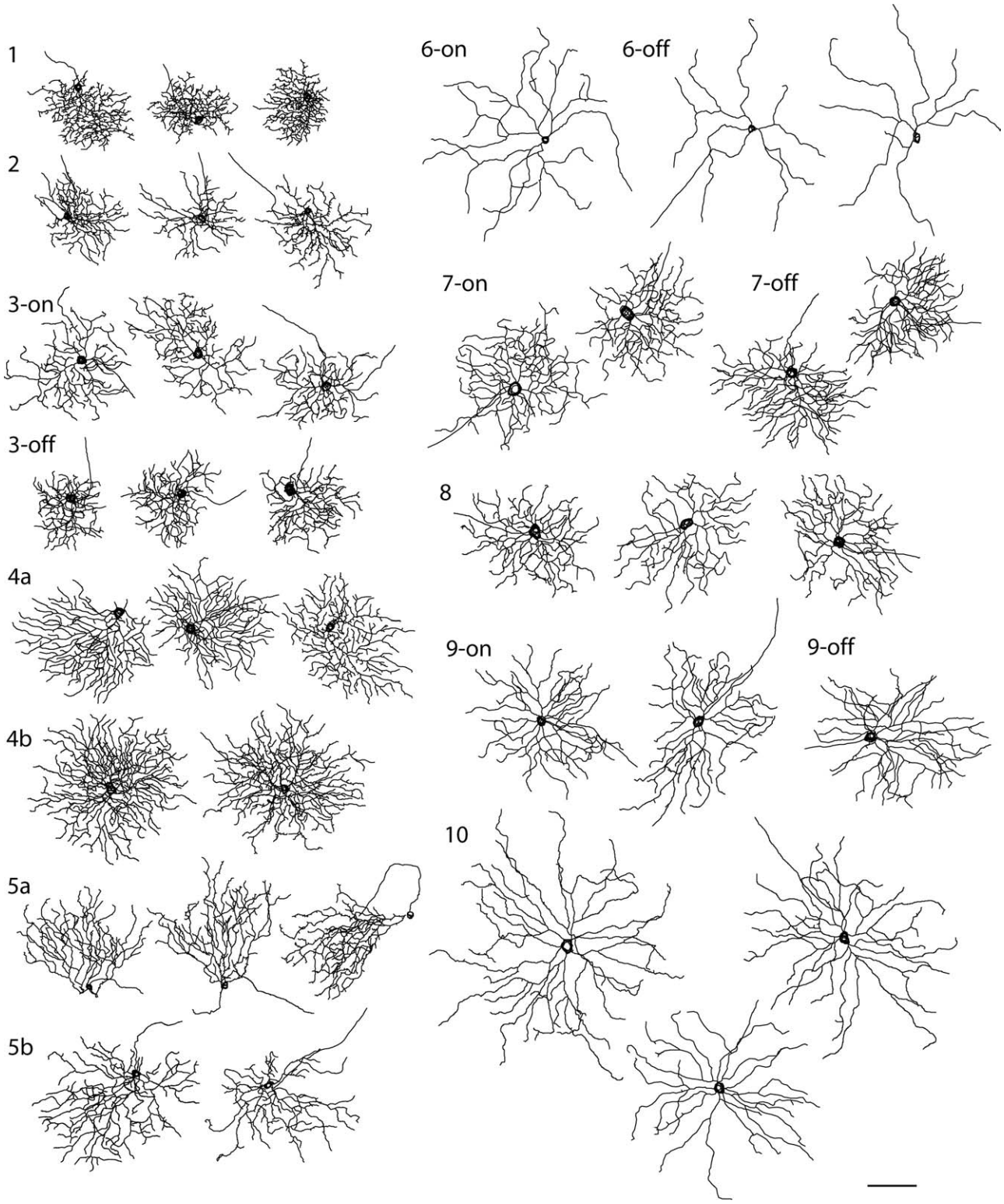

Fig. 2. Tracings of cells from the monostratified cell clusters. Examples of On and Off cells are shown for groups M3, M6, M7, and M9. For groups M4 and M5, examples of two different morphologies (a and b) found in each cluster are shown. All tracings are shown at same scale. Scale bar=100 μm.

were remarkably consistent for some of the clusters but more variable for others. For the monostratified cells (Fig. 7A), those in M5–M10 clusters had dendrites located close to one of the nuclear layers. Cells in M6, M9 and M10 had

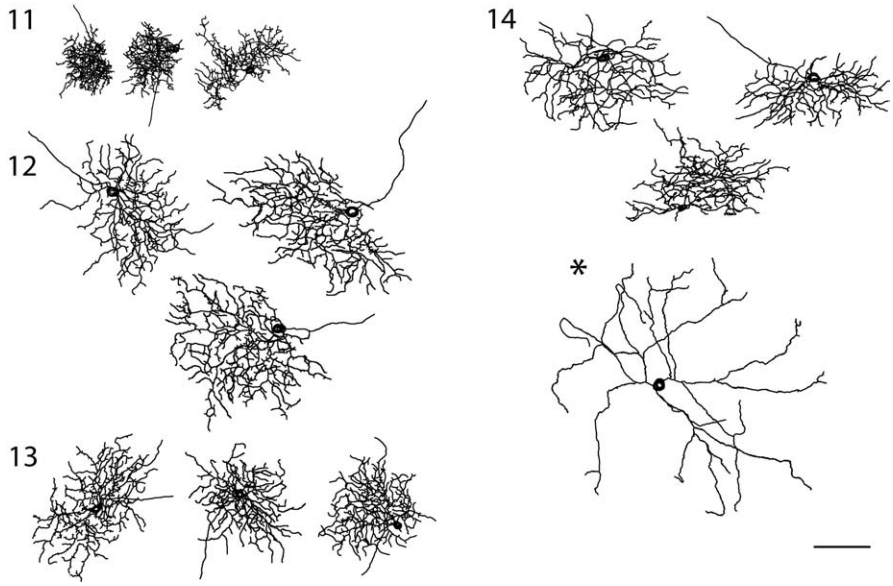

Fig. 3. Tracings of cells from the bistratified cell clusters. The asterisk shows a cell that was clustered by itself and thus was not given a group number. All tracings are shown at the same scale. Scale bar=100 μm.

their dendrites in layers 1 and 5, M7 in layers 2 and 5, M8 cell dendrites spanned layers 1, 2 and 4, 5, while those of M5 cells were in layers 1 and 4. Cells in clusters M1–M4 had dendrites located more centrally within the IPL, with the bulk of the dendrites of M1 and M4 cells stratifying in sublamina 3, near the On/Off border (gray dashed lines in Fig. 7A and B). The dendrites of both the On and Off cells of cluster M3 tended to stratify over a wider swath of the IPL, with the Off cells spanning across layers 1 and 2 and the bulk of the On cells spanning layers 4 and 5.

The loci of the dendrites of all the bistratified cells in clusters M11, 12, 13 and 14 are shown in Fig. 7B. Cells in cluster M11 tended to have a thick profusion of dendrites in layer 3 and a smaller, thinner spread in layer 1 (see Fig. 6). Cluster M12 cells had the largest dendritic fields and somas of all the bistratified cells, but the locations of their dendrites were similar to those of the cells in M13 (both had dendrites stratifying in layers 2 and 4). And, while M14 cells were similar to M13 cells in size, their dendrites tended to ramify closer to the nuclear layers, in layers 1 and 4 or 5.

Fig. 8 shows the means and standard errors of the 12 measurements, other than dendritic field and soma size, used to define the 14 cell clusters. Note that some cell

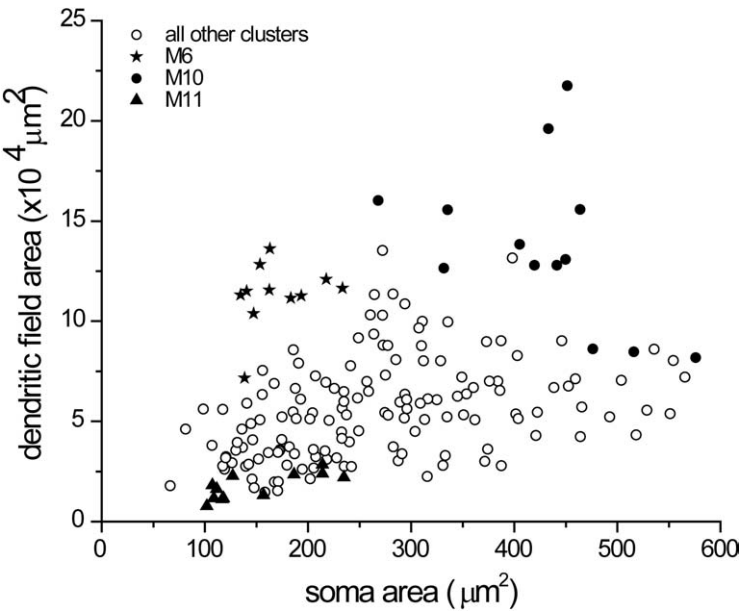

Fig. 4. Scatter plot of soma area vs. dendritic field area. Groups M6 (★), M10 (●), and M11 (▲) are compared with all other groups (○).

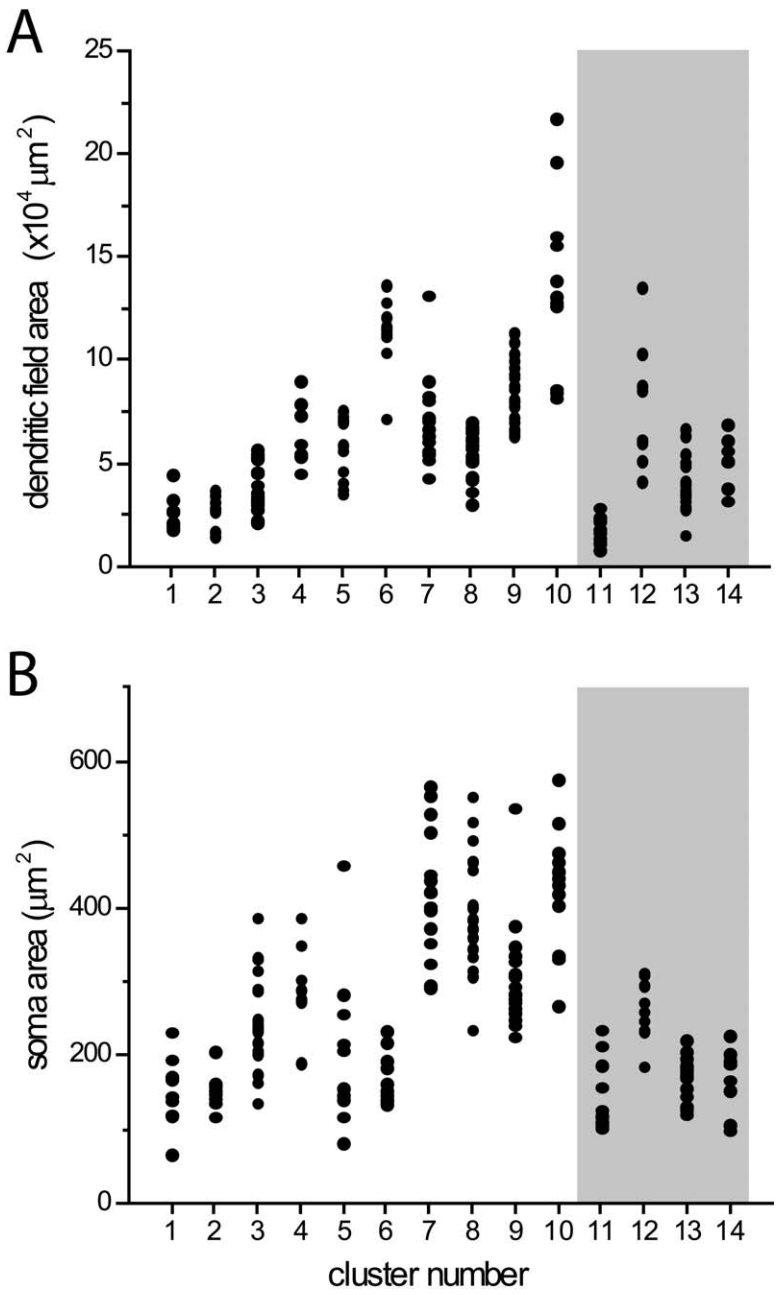

Fig. 5. Scatter plots of dendritic field (A) and soma area (B) for each group. The gray boxes highlight the bistratified cell clusters.

clusters were clearly distinguishable from all others on the basis a single parameter. For instance, M6 cells (including the melanopsin-positive cells) had terminal branch lengths that were much larger than any other cell type, cells in M5 showed the most asymmetry, and cells in M1 had the highest spine density. Clear-cut trends in branching patterns can also be seen. Thus, smaller cells had larger spine densities and tended to have dendrites located toward the middle of the IPL rather than at it edges (see Figs. 5 and 7). Smaller cells also tended to have smaller branch lengths, though there were exceptions to this trend, as can be seen by comparing clusters M4 and M8. Cells with longer mean branch lengths usually had smaller branch angles as well as larger dendrite and axon diameters.

There were also notable exceptions to these patterns; for example, M6 showed longer branch lengths than clusters M9 and 10, yet also had larger branch angles. The cells in M5 had longer branch lengths than those in M3 and M4 but also had thinner axon diameters. And, though cluster M7 had the thickest dendrites, the branches of these cells were of modest length. Collectively, these results show that while there are clear tendencies for certain parameters to co-vary, there are also exceptions to this trend that help to define the different cell groups.

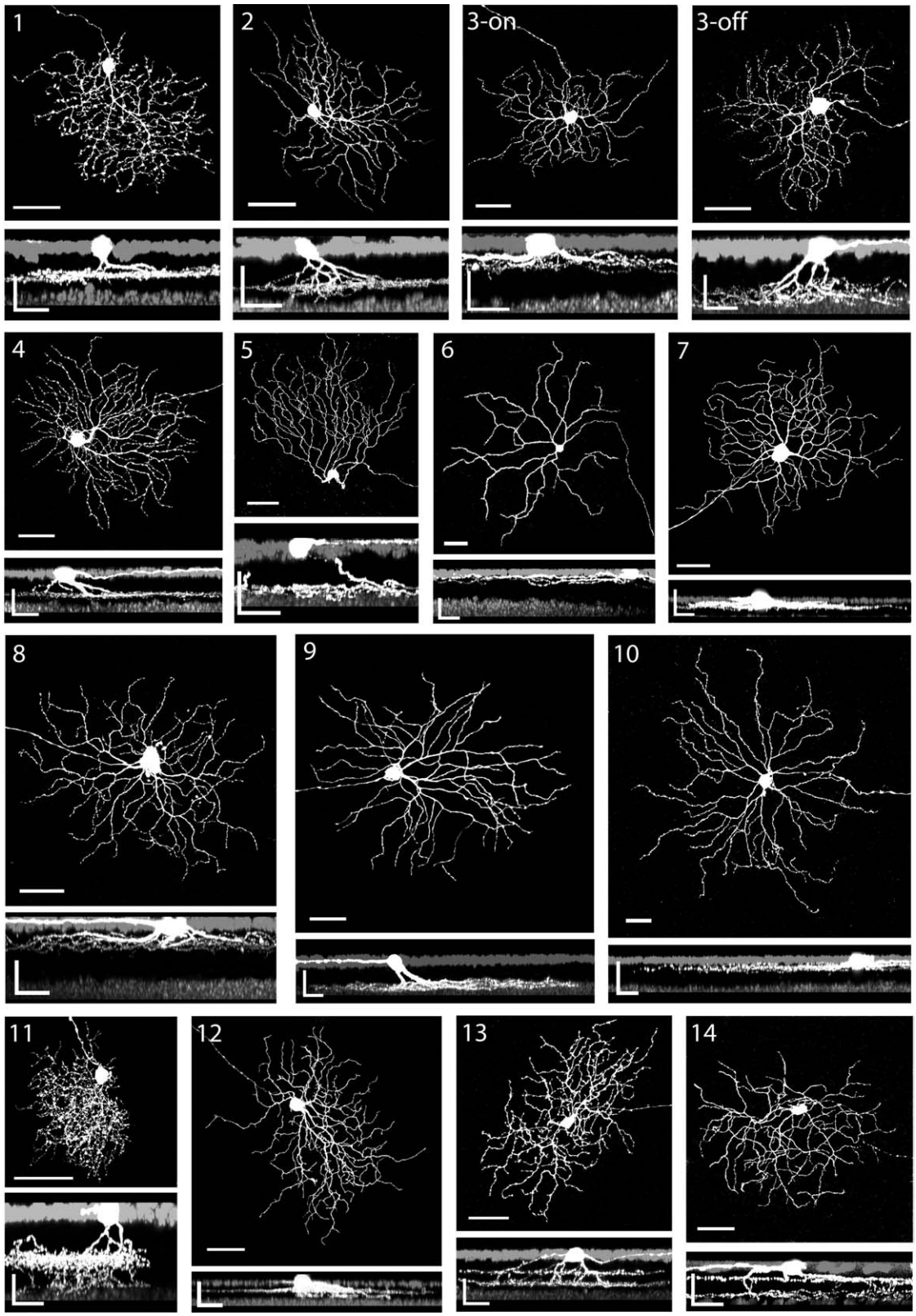

Fig. 6. Images of cells. Bird's-eye (XY plane) and side (XZ plane) views are shown for cells (top and bottom images respectively) from each cluster. The boundaries of the IPL are shown by the DAPI labeled nuclei (darker gray at the top, GCL, and the bottom, INL) in the side views. Tracings of these cells are shown in Figs. 2 and 3. Scale bars=50 μm.

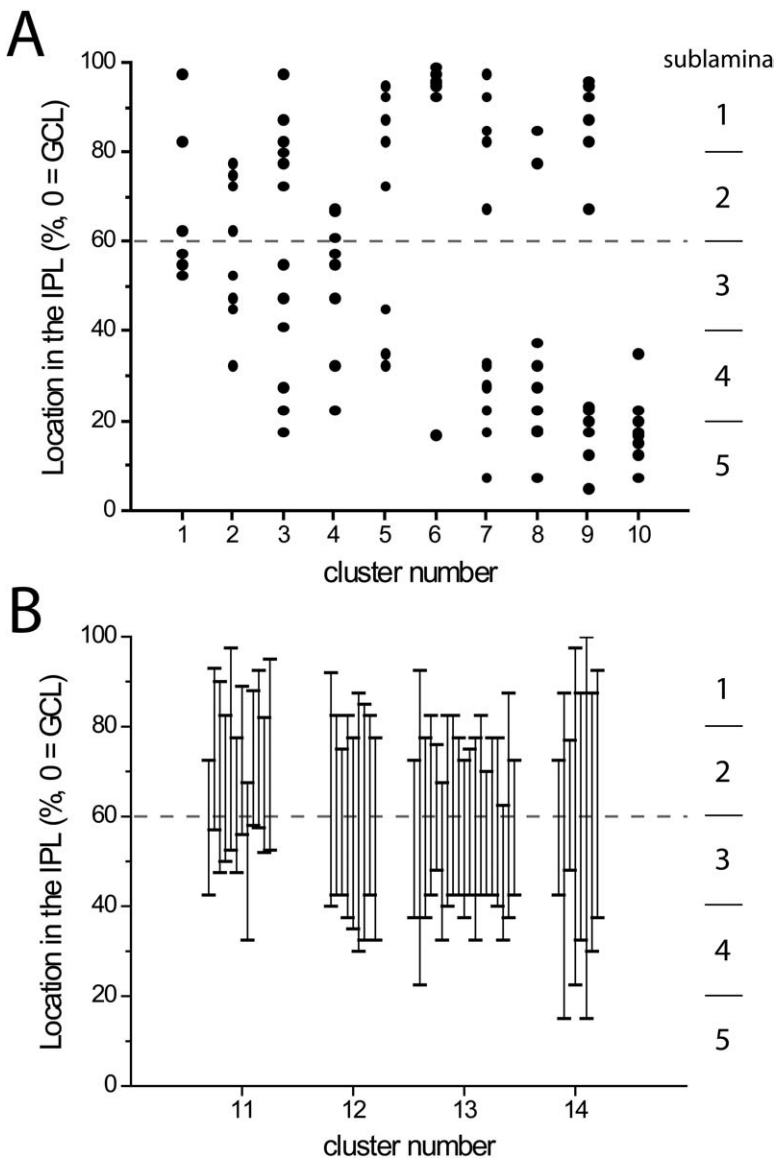

Fig. 7. Dendritic stratification patterns in the IPL. (A) Monostratified cells. The mean dendrite stratification depth is shown for the cells in each cluster. (B) Bistratified cells. Both the On and the Off mean stratification depths are shown for each cell in each cluster. Vertical lines connect the two dendrite locations for each bistratified cell. The presumed boundary between On and Off laminae is indicated by the dashed gray lines, with the sublaminae denoted on the right. GCL=0%; INL=100%.

Melanopsin-expressing cells

All of the cells recognized by the melanopsin antibody were placed into a single cluster, M6. These cells are all characterized by a small soma and a large, sparse dendritic field. We were able to visualize melanopsin-positive cells with dendrites stratifying only in layer 1. However, one other cell is included in this cluster, a YFP-expressing cell with a morphology indistinguishable from the cells recognized by the antibody but whose dendrites were located in layer 5 of the IPL. In addition, the one bistratified cell forming its own cluster (* in Fig. 1) was similar in appearance to the melanopsin-expressing cells. Thus, there appear to be three types of melanopsin cells in the mouse retina-On, Off, and On/Off.

SMI-32 positive cells

The antibody against neurofilament H (SMI-32) has been reported to label large ganglion cells with smooth dendrites in both the wild-type and genetically altered mouse retina (Lin et al., 2004). This suggested that SMI-32, like melanopsin, might label RGCs in a single cluster. However, we found that SMI-32 stained cells located in four different clusters. It should be noted that the methods, antibody vendor and antibody concentration we employed are the same as that used by Lin et al. (2004). Of the 11 cells labeled with SMI-32, two were clustered in M3, four in M7, two in M9 and three in M10. The cells in M9 and M10 had large dendritic fields and long dendritic branches as expected for alpha-like RGCs, but those in M3 and M7 did not. Exam-

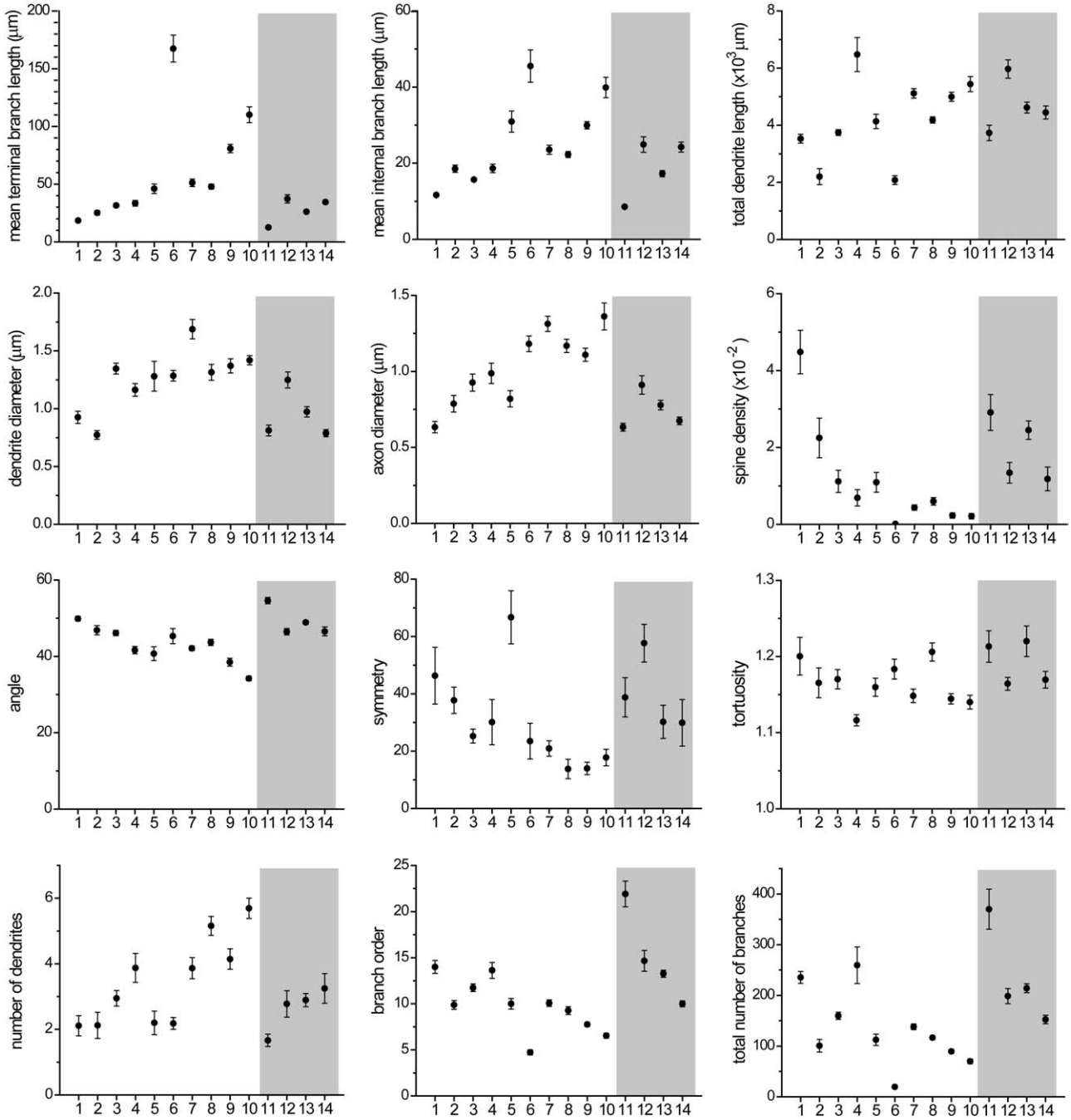

Fig. 8. Morphometric means per cluster. The mean values (±S.E.) for 12 of the 14 measurements included in the cluster analysis are plotted for each cluster. The gray boxes delineate the bistratified cell clusters.

ples of the different cell types labeled with this antibody are illustrated in Fig. 9. All of the SMI-32 positive cells had dendrites ramifying close to one of the nuclear layers.

YFP-expressing cells

All but one of the 14 clusters contained YFP expressing cells from the transgenic mice (see Table 1). Only cluster M11 did not contain any YFP-expressing cells. However, we did find a difference in the frequency and strength of expression between the clusters. Cells in M3, M8–M10, and M13 strongly expressed YFP, while cells in other clusters showed infrequent and weak YFP expression, which was enhanced by the use of an antibody against GFP.

DISCUSSION

Our sample of 182 mouse RGCs could be separated into 14 clusters, 10 with dendrites ramifying in either the On or Off sublaminae of the IPL and four with bistratified den-

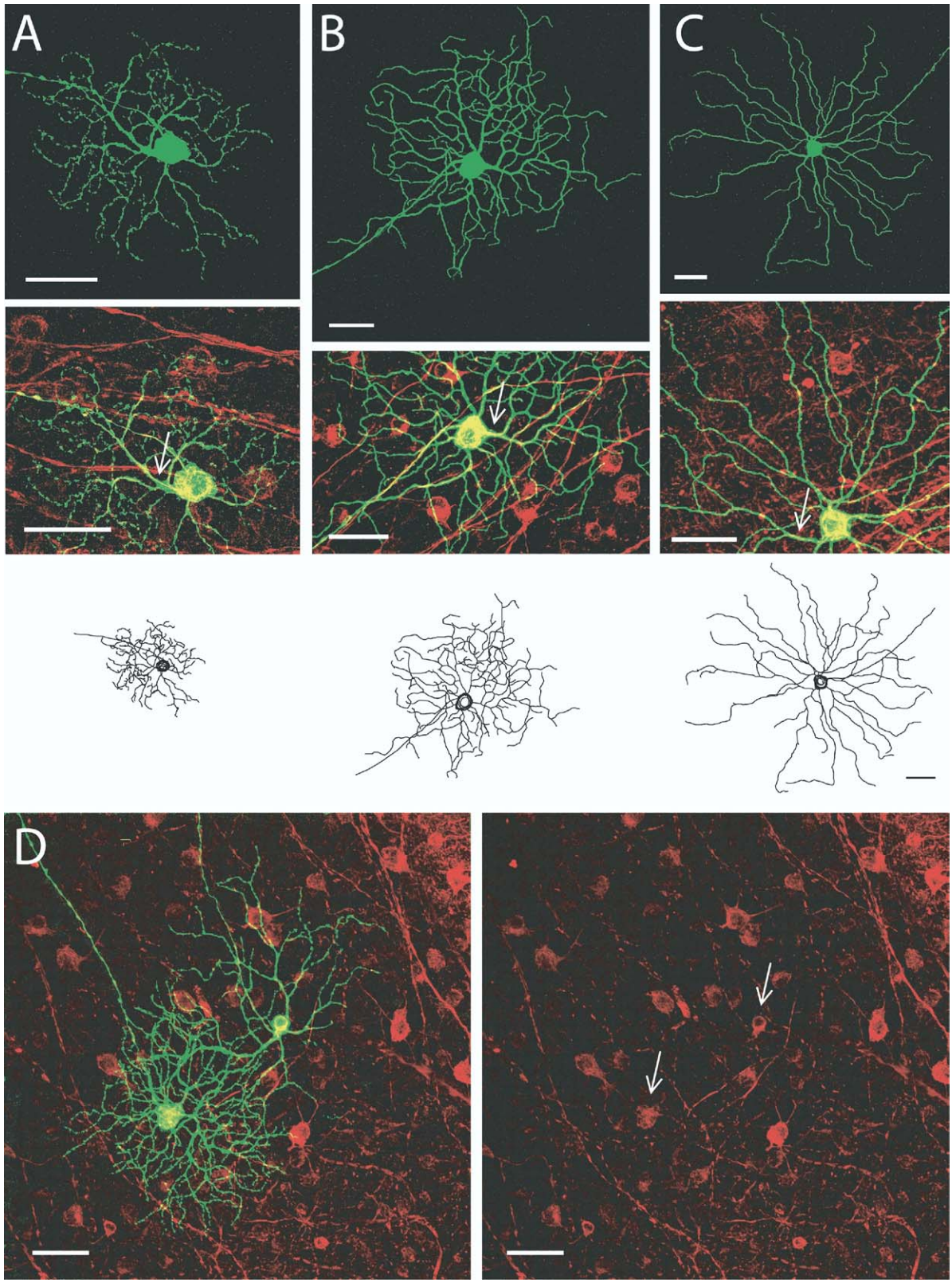

Fig. 9. SMI-32 antibody recognizes more than one type of mouse RGC. (A–C) SMI-32 label colocalizes with YFP-expressing RGCs from different clusters (A: cluster M3; B: M7; C: M10). Top images show RGC morphology. Middle images show the overlap (yellow) between the RGC (green) and SMI-32 (red). Arrows indicate SMI-32 label extending along dendrites. Bottom images are tracings of the cells shown above. Each image has its own scale bar; the tracings are drawn to a single scale bar shown at the bottom right in C. Scale bars=50 μm. (D) Left, two YFP-expressing cells that were also labeled with SMI-32 have distinct morphologies. The cells are representative of groups M7 and M9. Right, SMI-32 label is shown alone. The arrows point to the somas of the RGCs shown on the left. Scale bars=100 μm.

drites spanning these sublaminae. Though our data indicate that there may be two additional groups embedded in clusters M4 and M5, we suggest a total of 14 groups, rather than 16, because of the conditions of our analysis. Fourteen different parametric measures were included in the cluster analysis here. We chose to use this large number of measurements because it was not clear in advance which of them would be most useful in determining differences between cell groups. We also note that within the overall population many of these parameters covary, and thus may be redundant and increase the importance of some measures over others. However, as is evident in Fig. 8, trends seen in the overall population were not always duplicated between individual cell clusters. For instance, the internal and terminal branch lengths were highly correlated in the larger population, as one increased so did the other; but, for M2 vs. M3 and M5 vs. M7 and M8 (see Fig. 8), these closely related parameters violated the trend seen in the population as a whole. Thus, cell cluster identification was aided by the use of both branch length measures. Below, we summarize the most striking features of each cluster suggested by our analysis. As has been reported by others (Doi et al., 1995; Jeon et al., 1998; Sun et al., 2002b; Badea and Nathans, 2004), we did not see any appreciable variation in morphological properties with retinal location or eccentricity.

Of the monostratified cells, M1 neurons have the smallest dendritic fields; these stratify in layer 4 and have the highest spine densities. The dendritic fields and soma sizes of M2 cells are comparable to M1, but M2 cells stratify narrowly in layers 2 and 3, and the internal branch length of M2 cells is nearly twice that of M1 cells. M3 cells have small dendritic fields like M1 and M2 neurons, but have larger somas. M3 dendrites span layers 1 and 2 (Off) or 4 and 5 (On). As a group, M4 cells have medium-sized dendritic fields and somas and they tend to stratify in layer 3 of the IPL. Noteworthy features of this group are the large total dendrite lengths and large number of dendritic branches. M5 cells have the smallest somas of the medium-sized cells, with dendrites that tend to be asymmetrical. M6 contained all the melanopsin-positive RGCs, with the small somas and large dendritic fields characteristic of these cells. M7 and M8 neurons were similar with respect to soma size, branch length, and stratification depth, but the former were characterized by thicker and straighter dendrites with fewer primary processes. M9 cells have medium-sized somas and larger dendritic trees that stratified in either layer 1 (On) or layer 5 (Off). M10 cells have the largest somas, dendritic trees and axon diameters. These cells appear to correspond to alpha-like cells observed in other species (Peichl et al., 1987; Peichl, 1991).

Of the bistratified cells, M11 have the smallest and densest dendritic fields of all the cell clusters. Their dendrites ramify in layer 3, near the On/Off border and also, less extensively, in layer 1. M12 and M13 cells stratify in layers 2 and 4, but the dendritic fields of M12 neurons are larger and more asymmetric than those of M13 cells. The dendrites of cells in cluster M14 tend to be relatively straight with few branches that terminate in layer 1 as well as layers 4/5.

In species such as the cat and monkey, the major RGC classes with monostratified dendrites show pronounced morphological differences that are largely invariant with respect to the dendritic stratification pattern of these neurons. For instance alpha and beta cells in the cat retina are considered to be single classes and exhibit the same morphological properties irrespective of whether the dendrites terminate in the On or Off sublamina of the IPL (Peichl and Wässle, 1981; Wässle et al., 1981a,b). At the same time, in all species RGCs with bistratified dendrites have been found to exhibit functional properties distinct from those with monostratified dendrites. For these reasons, we relied on morphological criteria other than stratification levels to define distinct clusters of mouse RGCs for the monostratified and bistratified RGCs separately. This revealed that the 10 clusters of monostratified cells were characterized by relatively unique stratification patterns, whereas the dendritic stratification patterns of the four clusters of bistratified were relatively similar.

We used three different methods to label RGCs: intracellular filling with LY, gene gun (DiOlistics), and genetic insertion of fluorescent proteins, as well as labeling cells immunocytochemically. In our hands, these different approaches resulted in differential labeling of the cell clusters described here, with different clusters appearing predominantly with some methods compared with the others. For instance, the larger cells in M9 and M10 were well represented in the YFP-expressing retinas, while the smallest cells were seen most often using the gene gun. Moreover, there are also practical advantages and disadvantages inherent in these approaches. Injection of LY biased our sample toward cells with large somas and was labor intensive, but the filled cells were well isolated. DiOlistics labeled all cells types, but in many instances the dendrites of the labeled cells overlapped extensively, precluding their use in this study. Fluorescent proteins transgenically linked to a Thy-1 regulatory element have been used quite extensively for studies of mouse RGCs (Tian and Copenhagen, 2003; Lin and Masland, 2005) since their introduction as a neuronal marker by Feng et al. (2000), but prior to the present study it was unknown what proportion of mouse RGCs express these Thy-1-linked proteins. Our results indicate that YFP (in the YFP-H transgenic line) is expressed in all but one of the RGC clusters present in the mouse retina. Moreover, it is possible that some YFP-positive cells would be found in this cluster (M11) with an increased sample size. Thus, our findings indicate that YFP expression offers the best approach for obtaining a large number of representative mouse RGCs that are labeled sufficiently well to allow for quantitative assessment of morphological properties.

All the cells labeled with an antibody against mouse melanopsin were assigned to a single cluster (M6) in our analysis. However, the antibody directed against neurofilament H (SMI-32) labels more than one RGC cell type in the mouse. Specifically, RGCs in clusters M3, M7, M9 and M10 were stained with SMI-32. Thus, our data do not

Table 2. Comparison of M1–M14 with mouse RGC classes proposed by others

	Sun et al. (2002b)	Badea and Nathans (2004)	Kong et al. (2005)
Monostrat			
M1	B2, B4	1	
M2	B2, B4	1, 2	1
M3(on)			2, 4
M3(off)		3	3
M4a	C1		7
M4b			
M5a	C6	6	
M5b		8	
M6			
M7(on)	A2	9	5
M7(off)		3, 7	6
M8	A2	9	5
M9(on)	C2	7	8
M9(off)	A2	9	10
M10	A1	9	11
Bistrat			
M11	B2	4	
M12	D2	5, bi2	
M13	D1	5, bi1	
M14	D1	5, bi3	

We show provisional equivalencies based on the measurements available in the other works.

support the claim that SMI-32 is a specific marker of large ganglion cells in the mouse retina (Lin et al., 2004).

It would now be important to determine the functional properties of the 14 RGC clusters described here. To our knowledge, the only study addressing this issue is one describing the responses of three types of large RGCs to light stimulation in the mouse (Pang et al., 2003). Pang et al. (2003 describe three different physiological types of alpha-like RGCs in mouse, two Off and one On, noting that only a quarter of the responses they record are classically alpha-like (transient). Based on size descriptions, they recorded from cells that would be placed in our clusters M7 and M9, not M10 which were our largest cells. Peichl (1989) found that the Off-alpha cells in rat retina had much smaller dendritic fields than the On-alpha cells; if this is also true for mouse, the Off cells in M9 may represent Off-alpha cells. Moreover, a recent study by Nirenberg and colleagues (Carcieri et al., 2003) has revealed a number of functionally distinct ganglion cell classes using a cluster analysis approach based on multi-electrode recordings. Their results suggest at least five functional RGC classes based on their responses to flashed spots of light, but the morphological properties of these neurons remain to be identified.

Three recent studies have addressed the issue of mouse RGC identification based on morphology alone (Sun et al., 2002a; Badea and Nathans, 2004; Kong et al., 2005). Two of these studies relied on a cluster analysis approach to distinguish among different classes of mouse RGCs based on quantitative measurements of the salient structural properties of these neurons. Badea and Nathans (2004) used an AP reporter to visualize retinal neurons and multiple criteria to identify nine clusters of monostratified and three clusters of bistratifed RGCs, while Kong et al. (2005) labeled cells using three different methods and employed three parameters (level of stratification, extent of dendritic field and density of branching) to define 11 monostratified cell clusters.

Because different studies, including the present investigation, relied on different sets of criteria to classify mouse RGCs it is difficult to make direct comparisons among the proposed classification schemes. Nevertheless, certain similarities may be recognized, and both Badea and Nathans (2004) and Kong et al. (2005) provided a comparison of their clusters to the classes proposed by Sun et al. (2002a). In Table 2 we denote, where appropriate, the similarities between our proposed clusters and the designations provided previously. It should be noted, that all of the classifications available to date must be considered provisional.

The ultimate goal of classifying cells is to relate the morphological features of the different cell types to the expression of specific molecules. Our understanding of the molecular mechanisms controlling dendritic development is rapidly progressing (Wong and Ghosh, 2002; Aizawa et al., 2004; Akum et al., 2004; Yu and Malenka, 2004), so it seems reasonable to believe that we will soon be in position to relate the morphological diversity that characterizes M1 through M14 RGCs to specific programs of genetic control. Indeed, the mouse retina currently offers the optimal means for achieving this goal.

Acknowledgments—This work was supported by grants from the National Eye Institute of the NIH (EY03991, EY13301, and P20 MH6069) and the NIMH (P20 MH60975) as well from Research to Prevent Blindness.

REFERENCES

Aizawa H, Hu S-C, Bobb K, Balakrishnan K, Ince G, Gurevich I, Cowan M, Ghosh A (2004) Dendrite development regulated by CREST, a calcium-regulated transcriptional activator. Science 303:197–202.

Akum BF, Chen M, Gunderson SI, Riefler GM, Scerri-Hansen MM, Firestein BL (2004) Cypin regulates dendrite patterning in hippocampal neurons by promoting microtubule assembly. Nat Neurosci 7:145–152.

Amthor FR, Oyster CW, Takahashi ES (1983) Quantitative morphology of rabbit retinal ganglion cells. Proc R Soc Lond B 217: 341–355.

Badea TC, Nathans J (2004) Quantitative analysis of neuronal morphologies in the mouse retina visualized by using a genetically directed reporter. J Comp Neurol 480:331–351.

Belenky MA, Smeraski CA, Provencio I, Sollars PJ, Pickard GE (2003) Melanopsin retinal ganglion cells receive bipolar and amacrine cell synapses. J Comp Neurol 460:380–393.

Berson DM, Isayama T, Pu M (1999) The Eta ganglion cell type of cat retina. J Comp Neurol 408:204–219.

Berson DM, Pu M, Famiglietti EV (1998) The zeta cell: a new ganglion cell type in cat retina. J Comp Neurol 399:269–288.

Boycott BB, Wassle H (1974) The morphological types of ganglion cells of the domestic cat's retina. J Physiol 240:397–419.

Carcieri SM, Jacobs AL, Nirenberg S (2003) Classification of retinal ganglion cells: A statistical approach. J Neurophysiol 90:1704–1713.

Dacey DM, Peterson BB, Robinson FR, Gamlin PD (2003) Fireworks in the primate retina: in vitro photodynamics reveals diverse LGN-projecting ganglion cell types. Neuron 37:15–27.

Doi M, Uji Y, Yamamura H (1995) Morphological classification of retinal ganglion cells in mice. J Comp Neurol 356:368–386.
Feng G, Mellow RH, Bernstein M, Keller-Peck C, Nguyen QT, Wallace M, Nerbonne JM, Lichtman JW, Sanes JR (2000) Imaging neuronal subsets in transgenic mice expressing multiple spectral variants of GFP. Neuron 28:41–51.
Gan WB, Grutzendler J, Wong WT, Wong RO, Lichtman JW (2000) Multicolor 'DiOlistic' labeling of the nervous system using lipophilic dye combinations. Neuron 27:219–225.
Huxlin KR, Goodchild AK (1997) Retinal ganglion cells in the albino rat: revised morphological classification. J Comp Neurol 385:309–323.
Isayama T, Berson DM, Pu M (2000) Theta ganglion cell type of cat retina. J Comp Neurol 417:32–48.
Jeon C-J, Strettoi E, Masland RH (1998) The major cell populations of the mouse retina. J Neurosci 18:8936–8946.
Kaplan E (2004) The M, P, and K pathways of the primate visual system. In: The visual neurosciences (Chalupa LM, Werner JS, eds), pp 481–493. Cambridge, MA: MIT Press.
Kolb H, Nelson R, Mariani A (1981) Amacrine cells, bipolar cells and ganglion cells of the cat retina: A Golgi study. Vision Res 21: 1081–1114.
Kong JH, Fish DR, Rockhill RL, Masland RH (2005) Diversity of ganglion cells in the mouse retina: Unsupervised morphological classification and its limits. J Comp Neurol 489:293–310.
Leventhal AG, Rodieck RW, Dreher B (1985) Central projections of cat retinal ganglion cells. J Comp Neurol 237:216–226.
Lin B, Masland RH (2005) Synaptic contacts between an identified type of ON cone bipolar cell and ganglion cells in the mouse retina. Eur J Neurosci 21:1257–1270.
Lin B, Wang SW, Masland RH (2004) Retinal ganglion cell type, size, and spacing can be specified independent of homotypic dendritic contacts. Neuron 43:475–485.
Marc RE, Jones BW (2002) Molecular phenotyping of retinal ganglion cells. J Neurosci 22:413–427.
Pang JJ, Gao F, Wu SM (2003) Light-evoked excitatory and inhibitory synaptic inputs to ON and OFF alpha ganglion cells in the mouse retina. J Neurosci 23:6063–6073.
Peichl L (1989) Alpha and delta ganglion cells in the rat retina. J Comp Neurol 286:120–139.
Peichl L (1991) Alpha ganglion cells in mammalian retinae: Common properties, species differences, and some comments on other ganglion cells. Vis Neurosci 7:155–169.
Peichl L, Ott H, Boycott BB (1987) Alpha ganglion cells in mammalian retinae. Proc R Soc Lond B 231:169–197.
Peichl L, Wässle H (1981) Morphological identification of on- and off-centre brisk transient (Y) cells in the cat retina. Proc R Soc Lond B 212:139–156.
Perry VH (1979) The ganglion cell layer of the retina of the rat: a Golgi study. Proc R Soc Lond B 204:363–375.
Perry VH, Cowey A (1984) Retinal ganglion cells that project to the superior colliculus and pretectum in the macaque monkey. Neuroscience 12:1125–1137.
Perry VH, Oehler R, Cowey A (1984) Retinal ganglion cells that project to the dorsal lateral geniculate nucleus in the macaque monkey. Neuroscience 12:1101–1123.
Provencio I, Rodriguez IR, Jiang G, Hayes WP, Moreira EF, Rollag MD (2000) A novel human opsin in the inner retina. J Neurosci 20:600–605.
Rockhill RL, Daly FJ, MacNeil MA, Brown SP, Masland RH (2002) The diversity of ganglion cells in a mammalian retina. J Neurosci 22:3831–3843.
Rodieck RW, Watanabe M (1993) Survey of the morphology of macaque retinal ganglion cells that project to the pretectum, superior colliculus, and parvicellular laminae of the lateral geniculate nucleus. J Comp Neurol 338:289–303.
Saito H-A (1983) Morphology of physiologically identified X-, Y-, and W-type retinal ganglion cells of the cat. J Comp Neurol 221: 279–288.
Stone J, Clarke R (1980) Correlation between soma size and dendritic morphology in cat retinal ganglion cells: Evidence of further variation in the γ-cell class. J Comp Neurol 192:211–217.
Sun W, Li N, He S (2002a) Large-scale morphological survey of mouse retinal ganglion cells. J Comp Neurol 451:115–126.
Sun W, Li N, He S (2002b) Large-scale morphological survey of rat retinal ganglion cells. Vis Neurosci 19:483–493.
Tian N, Copenhagen DR (2003) Visual stimulation is required for refinement of ON and OFF pathways in postnatal retina. Neuron 39:85–96.
Vitek DJ, Schall JD, Leventhal AG (1985) Morphology, central projections, and dendritic field orientation of retinal ganglion cells in the ferret. J Comp Neurol 241:1–11.
Wässle H, Boycott BB, Illing R-B (1981a) Morphology and mosaic of on- and off-beta cells in the cat retina and some functional considerations. Proc R Soc Lond B 212:177–195.
Wässle H, Peichl L, Boycott BB (1981b) Morphology and topography of on- and off-alpha cells in the cat retina. Proc R Soc Lond B 212:157–175.
Wingate RJT, Fitzgibbon T, Thompson ID (1992) Lucifer Yellow, retrograde tracers, and fractal analysis characterise adult ferret retinal ganglion cells. J Comp Neurol 323:449–474.
Wong ROL, Ghosh A (2002) Activity-dependent regulation of dendritic growth and patterning. Nat Rev Neurosci 3:803–812.
Yu X, Malenka RC (2004) β-Catenin is critical for dendritic morphogenesis. Nat Neurosci 6:1169–1177.

(Accepted 8 February 2006)
(Available online 19 April 2006)